Mutual information discloses relationship between hemodynamic variables in artificial heart-implanted dogs

MOTOHISA OSAKA, TOMOYUKI YAMBE, HIROKAZU SAITOH, MAKOTO YOSHIZAWA, TAKASHI ITOH, SHIN-ICHI NITTA, HIROSHI KISHIDA, AND HIROKAZU HAYAKAWA
First Department of Internal Medicine and Center of Informatics Science, Nippon Medical School, Tokyo 113–8603; Department of Medical Engineering and Cardiology, Division of Organ Pathology, Institute of Development, Aging, and Cancer, and Department of Electrical Engineering, Faculty of Engineering, Tohoku University, Sendai 980–8575, Japan

Osaka, Motohisa, Tomoyuki Yambe, Hirokazu Saitoh, Makoto Yoshizawa, Takashi Itoh, Shin-Ichi Nitta, Hiroshi Kishida, and Hirokazu Hayakawa. Mutual information discloses relationship between hemodynamic variables in artificial heart-implanted dogs. *Am. J. Physiol.* 275 (*Heart Circ. Physiol.* 44): H1419–H1433, 1998.—A mutual information (MI) method for assessment of the relationship between hemodynamic variables was proposed and applied to the analysis of heart rate (HR), arterial blood pressure (BP), and renal sympathetic nerve activity (RSNA) in artificial heart-implanted dogs to quantify correlation between these parameters. MI measures the nonlinear as well as linear dependence of two variables. Simulation studies revealed that this MI technique furnishes mathematical features well suited to the investigation of nonlinear dynamics such as the cardiovascular system and can quantify a relationship between two parameters. To constitute a model free of the natural heart, two pneumatically actuated ventricular assist devices were implanted as biventricular bypasses in acute canine experiments. RSNA was detected with the use of bipolar electrodes attached to the renal sympathetic nerve. Analysis of data during control revealed that correlation between HR and RSNA was higher than that between HR and BP and that between RSNA and BP ($P < 0.05$). Although RSNA seemed to fluctuate noncorrelatedly with BP in higher pacing rates, the MI values between them disclosed their strong correlation. Surprisingly, correlation between RSNA and BP was stronger during a pacing rate of 60 beats/min than during higher pacing rates and control ($P < 0.05$). It is suggested that the baroreflex system may be susceptible to pacing rates during the total artificial heart state. We calculated the time delay between HR and RSNA, between RSNA and BP, and between HR and BP by regarding a time delay at which the maximum MI value between each pair of parameters was given as a physiological delay. Our results indicate that RSNA leads BP, BP leads HR, and RSNA leads HR during control ($P < 0.05$). We conclude that this method could provide a powerful means for measuring correlation of physiological variables.

cardiovascular regulation; autonomic nervous system; nonlinear dynamics; spectral analysis; computer simulation

CONVENTIONAL ANALYSES of the correlation of two time series, such as cross-correlation function in the time domain and coherency in the frequency domain, have been widely used (2, 9, 10, 28, 30, 31). For linear systems, the coherency function $C(\omega)$ between $x(t)$ and $y(t)$ can be interpreted as the fractional portion of the mean-square value at $y(t)$ that is contributed by $x(t)$ at a frequency ω. Conversely, the quantity $1 - C(\omega)$ is a measure of the mean-square value of $y(t)$ when $x(t)$ is not accounted for at the frequency ω (Ref. 7, p. 172). However, it does not provide any information about whether they are nonlinearly correlated. Hence, these techniques are inappropriate to assess nonlinear dynamics. On the other hand, it has been demonstrated that the cardiovascular system comprises nonlinear dynamics from micro to macro in scope (5, 17, 19, 25). In particular, beat-to-beat heart rate variability has been proven to contain an appreciable amount of fractal components in the time series (11, 36). Hence, a new measure is needed to quantify the correlation between various hemodynamic parameters.

Mutual information (MI), to be defined precisely later, can measure the nonlinear as well as linear dependence of two variables. This method has been proposed to provide a good criterion for the choice of time delay in phase-portrait reconstruction from time series by gauging correlation between an original series and its delayed series (15). MI can provide a quantitative characterization of chaotic spatial patterns. Moreover, MI analysis is also applicable to the detection of nonlinearity of time series (29). We previously applied MI to the assessment of patterns of occurrence of ventricular premature beats and reported that the method can quantify randomness of their occurrence (26). Thus we think this method could be applied to quantify the relationship between various hemodynamic parameters.

The power spectrum analysis of heart rate (HR) or arterial blood pressure (BP) variability has been widely recognized as a useful means for evaluating the autonomic balance noninvasively (2, 3, 6, 9, 10, 23, 25, 27, 28, 30–32). The low-frequency spectra have been generally thought to reflect the sympathetic activity with the parasympathetic modulation and the high-frequency spectra to reflect the parasympathetic activity modulated by respiration. However, a direct relationship between sympathetic activity and either HR or BP in the low-frequency spectra has been controversial recently (1, 6, 10, 28). One of the reasons for this is that determination of the origin of the rhythmic fluctuations in the circulatory system is very difficult because there are some interactions between hemodynamic parameters. For example, BP influences HR through the baroreflex, which combines the effects of the afferent signal from BP to the vasomotor center and the efferent

The costs of publication of this article were defrayed in part by the payment of page charges. The article must therefore be hereby marked "*advertisement*" in accordance with 18 U.S.C. Section 1734 solely to indicate this fact.

signals of the sympathetic and parasympathetic nerves to the sinus node. HR affects BP through the mechanical coupling between the left ventricle and the vasculature. Thus we thought that an open-loop identification analysis might be a potential choice for investigating the origin of these fluctuations. The use of a totally artificial heart should allow an open-loop analysis of the cardiovascular system with respect to the heart. Moreover, the artificial heart, including ventricular assist devices, which can return patients with congestive heart failure to society, will be in great demand. Although a number of control algorithms and strategies for driving the artificial heart have been described during the last two decades, current control methods are based on information such as hemodynamics, oxygen utilization, and hormonal factors (4, 21, 22). However, reports on evaluation of the autonomic nervous system in the artificial heart are still sparse. It is obvious that the circulatory control system including the baroreflex system must be carefully investigated to determine the optimal driving conditions for the artificial heart from a neurophysiological point of view.

We sought to refine the MI analysis to assess the relationship among HR, renal sympathetic nerve activity (RSNA), and BP. The purpose of this study was to propose and test a new method based on MI that could be applied to hemodynamic data and that could assess alterations in neurocardiovascular interactions in a variety of physiological conditions. To test our new technique, we first examined its validity with simulated data and then evaluated its reliability with data from dogs during control and during the driven complete artificial circulation.

METHODS

General Procedure

The experimental protocol was approved by the Tohoku University Committee on Animal Care. Seven adult mongrel dogs of both sexes, weighing 15–35 kg, were anesthetized by intravenous thiopental sodium (2.5 mg/kg) and ketamine sodium (5.0 mg/kg) administration and nitrous oxide inhalation under mechanical ventilation. Experimental preparations are shown in Fig. 1. After tracheal tube intubation, the animals were placed on a volume-limited respirator (ARF-850, Acoma, Tokyo, Japan). Electrodes for electrocardiograms were implanted in the left foreleg and both hind legs.

After the left pleural cavity was opened through the fifth intercostal space, the pericardium was partially incised to expose the left atrium. Aortic pressure and left atrial pressure (LAP) were monitored continuously by catheters inserted into the aorta and left atrium through the left femoral artery and the left appendage, respectively. For left artificial heart implantation, the intercostal arteries were dissected to free the descending aorta. A polyvinyl chloride outflow cannula with a T-shaped pipe was inserted into the descending aorta and secured with a ligature. An inflow cannula was inserted into the left atrium through the left atrial appendage. Both cannulas were connected to the authors' TH-7B pneumatically driven sac-type blood pump via the built-in valve connectors (37, 38). An outflow cannula was inserted into the pulmonary artery, and an inflow cannula was inserted into the right atrium through the right atrial appendage. Both cannulas were connected to the right pump. After the driving

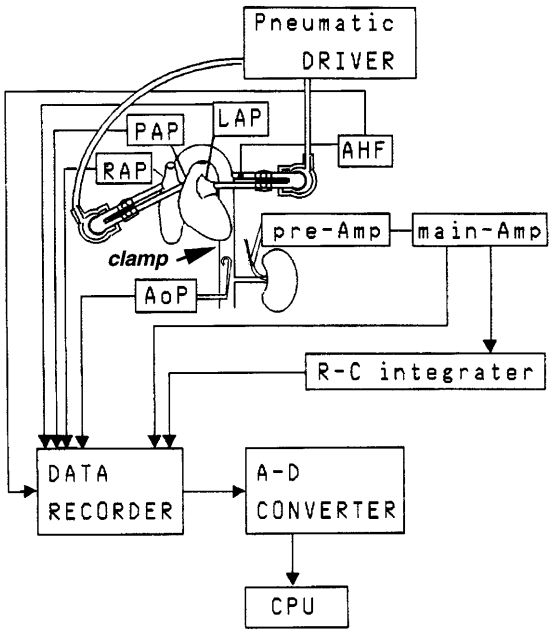

Fig. 1. Schematic drawing of the experimental system. Arrow labeled "clamp" indicates site where descending aorta was clamped to identify the observed signal as sympathetic nerve discharge. A/D, analog to digital; AHF, artificial heart flow; AoP, aortic pressure; LAP, left atrial pressure; main-Amp, main amplifier; pre-Amp, preamplifier; PAP, pulmonary artery pressure; RAP, right atrial pressure; R-C, resistance-capacitance.

of both pumps was initiated, ventricular fibrillation was electrically induced. After ventricular fibrillation was induced, we observed that the pulse-synchronous discharges in the RSNA did not change their periodicity and quantity significantly. With respect to the influence of the fibrillated heart on RSNA, Toda et al. (34) reported that the fibrillated heart had little influence on the RSNA and was presumably not essential for maintaining nervous control of circulation as long as the circulation was maintained by an artificial heart.

The pumps were driven by a pneumatic drive console that we developed (24). The positive and negative pressure and systolic duration of both blood pumps were selected to maintain hemodynamic derivatives within the control range: mean aortic pressure was maintained within 60–140 mmHg, mean LAP within 5–12 mmHg, mean pulmonary artery pressure <30 mmHg, and right atrial pressure <5 mmHg (Fig. 1). Pump output was controlled to maintain a cardiac output similar to that during the control state.

Recording of Nerve Activity

The left flank was opened between the iliac crest and the costovertebral angle, and the left renal artery was then exposed. The left renal sympathetic nerve bundle was separated from the left renal artery and surrounding connective tissues. After the nerve sheath was removed, the nerve was placed on bipolar stainless steel electrodes for recording of RSNA. The renal sympathetic nerve discharges were led into a preamplifier with a gain of 1,000 and an amplifier with a gain of 50 (DPA-21 and DPA-11E, DIA Medical System, Tokyo, Japan). Amplified signals were routed through a band-pass filter with a bandwidth of 30–3,000 Hz and through an amplitude discriminator to a storage oscilloscope. For analysis, the filtered neurogram was integrated by a resistance-capacitance circuit with a time constant of 0.1 s.

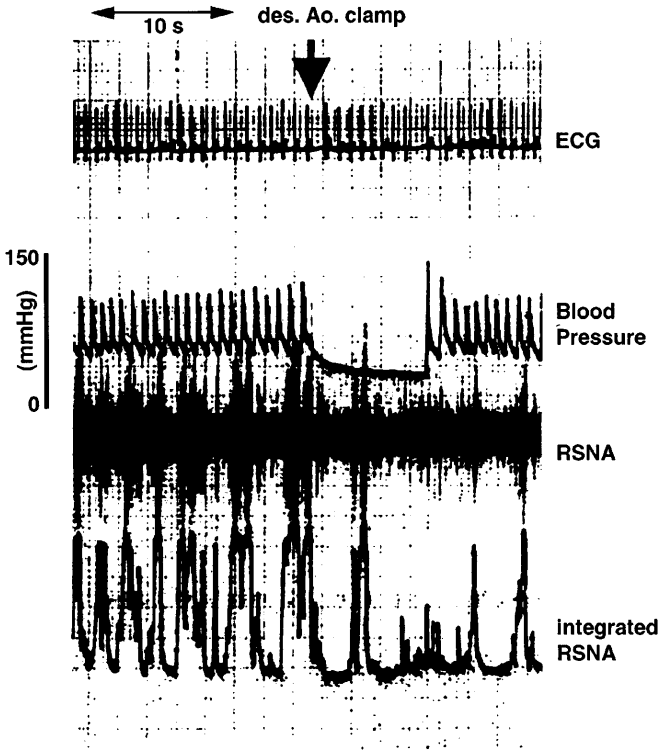

Fig. 2. Identification of sympathetic nerve discharge by clamping descending aorta (des Ao) transiently above level of renal arteries, as indicated in Fig. 1. During clamp, renal sympathetic nerve activity (RSNA) decreased because arterial blood pressure (BP) increased at aortic arch. The reason for the abrupt decrease in BP is that a catheter for measuring BP was left below the clamping site.

To identify the observed signal as the sympathetic nerve discharge, we transiently clamped the descending aorta above the level of the renal arteries, as indicated in Fig. 1. During the clamp RSNA decreased rapidly because BP increased at the aortic arch (Fig. 2). However, the reason why BP decreased abruptly in Fig. 2 is that a catheter to measure BP was left below the clamping site. We confirmed that the respiratory rhythm of RSNA was changed significantly in accordance with the changes in the respiratory rhythm of the mechanical ventilator (14). Figure 3 shows the recording from the natural heart state to a stationary state of biventricular bypass circulation after electrical induction of ventricular fibrillation. Careful inspection of Fig. 3 suggests a reciprocal relationship between RSNA and BP; that is, RSNA bursts occurred primarily when BP was falling, whereas there was little RSNA when BP was increasing. When the nerve discharge signal was significantly contaminated by environmental electromagnetic noise, the animal was covered with wire netting to avoid production of the noise.

Data Analysis

The signals of hemodynamic parameters and sympathetic nerve activity were recorded with an ink-jet recorder and on magnetic tape after the stabilization of all hemodynamic derivatives (almost 20–30 min after the preparation). After the control data were recorded, ventricular fibrillation was induced electrically. Time series were recorded in a stationary state of the hemodynamics during the different pacing rates from 60 to 160 beats/min. These data were played back from the magnetic tape.

The occurrence of R waves was detected in each record, and a smoothed instantaneous HR time series was constructed and sampled at 8 Hz using the algorithm proposed by Berger

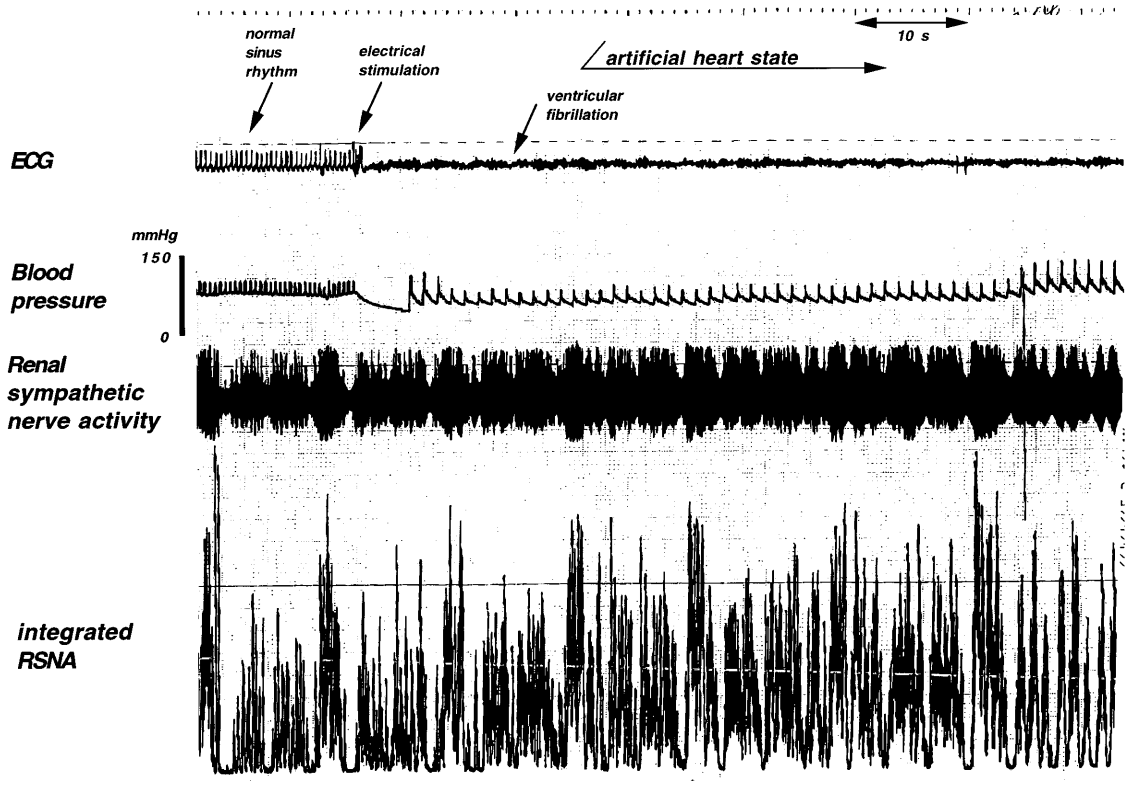

Fig. 3. Recording of electrocardiogram (ECG), BP, RSNA, and integrated RSNA. After electrical induction of ventricular fibrillation, driving of both artificial pumps was initiated. It took ~1 min to adjust driving condition until cardiac output was maintained.

et al. (8). All R-R intervals during control were measured at an accuracy of 1 ms. A time series of R-R intervals that comprised only beats in normal sinus rhythms and in a stationary state was selected for the final analysis.

A time series of BP was constructed as that of arterial blood pressure averaged from beat to beat. Time series of BP and RSNA were splined and sampled at 8 Hz so that values of all the constructed time series occurred simultaneously.

MI Analysis

We calculated MI values according to an algorithm proposed by Fraser and Swinney (15). For a couple of time series, $x(t)$ and $y(t)$, we measured the dependency of the values of $y(t + T)$ on the values of $x(t)$, where T was a time delay and data length was the power of two. We made the assignment $(s, q) = [x(t), y(t + T)]$ to consider a general coupled system (S, Q). MI of this system $[I(S, Q)]$ is defined as the answer to the question, "Given a measurement of s, how many bits on the average can be predicted about q?"

$$I(S, Q) = \int P_{sq}(s, q) \log [P_{sq}(s, q)/[P_s(s)P_q(q)]]\mathrm{d}s\mathrm{d}q$$

where S and Q denote the systems; $P_s(s)$ and $P_q(q)$ are the probability densities at s and q, respectively; and $P_{sq}(s, q)$ is the joint probability density at s and q. The larger the value of MI is for (S, Q), the stronger the mutual dependence is between S and Q. The algorithm of MI will be described in APPENDIX A.

We denote time series of HR, RSNA, and BP as HR(t), RSNA(t), and BP(t), respectively. The data length was between 2^9 and 2^{11} samples, that is, between 64 and 256 s, because the data were sampled at 8 Hz. If $S = Q$, the correlation between them should be perfect, and then $I(S, Q) = n$, where the data length is 2^n, because the algorithm is developed to the discrete case. This point will be discussed in APPENDIX A. The MI value between the same two time series is n. Hence, MI values were normalized by n; in other words, these values were divided by n. We calculated mutual information $I(T)$ of (S, Q), where S is a time series of HR(t), RSNA(t), or BP(t) and Q is another time series with a time delay T; for example, S = HR(t) and Q = RSNA($t + T$). T was then between -5 and 5 s in a step of 0.125 s. The maximum value of $I(T)$ between S and Q, where T was from -5 to 5 s, is denoted by $I_{max}(S, Q)$. We considered a time delay $T_{max}(S, Q)$, at which the maximum value of $I(T)$ of (S, Q) was given, as a physiological delay between these parameters. The definition of $T_{max}(S, Q)$ will be discussed later (see DISCUSSION). If $T_{max}(S, Q)$ is negative, then S leads Q, and if $T_{max}(S, Q)$ is positive, vice versa.

Coherency Analysis

To compare MI analyses, we calculated coherency among HR, RSNA, and BP. Ordinary coherence function estimates were computed as the ratio of the magnitude square of the cross spectra divided by the product of the autospectra. Coherence is a measure of the statistical link between two variability series at any given frequency and is expressed as a number between zero and one. The significant value of coherency will be discussed in *Simulation 4*. The confidence in spectral estimates can be enhanced by dividing data into multiple epochs and ensemble averaging. Although this decreases variance and increases confidence, it reduces resolution because a reciprocal of the length of the data epoch determines the limits of the low-frequency resolution. Auto- and cross-spectra estimates were optimized by ensemble averaging between 9 and 31 data epochs of 128 points (16 s) using Welch's method (7). To reduce the loss of stability, the original data were sectioned using a 50% overlap. Before a fast Fourier algorithm was used, linear trends were removed from the data, and data were tapered with the use of a Hanning window.

Statistical Procedures

Values of continuous variables are presented as means ± SE. We used nonparametric two-way ANOVA (Friedman's test) to test for statistical significance between the various stages of the experimental study. A two-tailed $P < 0.05$ was considered significant.

RESULTS

Simulation Studies

Simulation 1. To demonstrate an effect of noise added to original simulated data on MI values between the original time series and its noisy series, a couple of time series were generated with noise according to the following formulas (29)

$$x(t) = [R_1 + R_2 \sin (2\pi f_2 t + \phi)] \sin (2\pi f_1 t)$$

$$y(t) = [R_1 + R_2 \sin (2\pi f_2 t + \phi)] \sin (2\pi f_1 t) + \xi$$

where $R_1{:}R_2$ = 5:4, $f_1{:}f_2$ = 10:9, $\phi = 1.3\pi$, and ξ are random numbers uniformly distributed between $-\Gamma$ and Γ. These time series were sampled at 10 Hz. The term "50% noise" means that $R_1{:}R_2{:}\Gamma$ = 5:4:9. The time series $x(t)$ represents the torus series without noise. A torus series such as $x(t)$ is a simple example of a nonlinear and yet periodic series. We considered it appropriate to compare the reliability of MI analysis with that of coherency analysis. With the percentage of noise increasing, peaks at several main frequencies will be obscured in the power spectrum of the noise-contaminated torus series. Hence, there is considered to be no significant correlation between the original torus series and noisy series that do not show any characteristic spectra due to the two fundamental frequencies (f_1 and f_2). This is why it was chosen to determine a threshold value of MI to detect a significant correlation.

$I[x(t), y(t)]$ were computed from an original torus series and noisy torus series that were 1,024 samples long and contained 10–90% noise. For each percentage of noise, 10 sets of $I[x(t), y(t)]$ were computed by generating different seeds of random numbers 10 times. $I[x(t), y(t)]$ at 10, 20, ..., 90% noise were compared by one-way factorial ANOVA. Figure 4 shows that the MI value decreased with an increasing percentage of noise ($P < 0.0001$). For frequency analysis, these data were sectioned using a 50% overlap, and auto- and cross-spectra estimates were optimized by ensemble averaging 15 data epochs of 128 points. Because the ratio f_1/f_2 of the two fundamental frequencies (f_1 = 1.59 Hz and f_2 = 1.43 Hz) is rational, all the peaks are harmonics of the frequency $f = f_1 - f_2$ (0.16 Hz) in the power spectrum of $x(t)$. Because the three main peaks in the spectrum of $x(t)$ became obscure in the spectrum of noisy torus $y(t)$ containing >80% noise, the average of

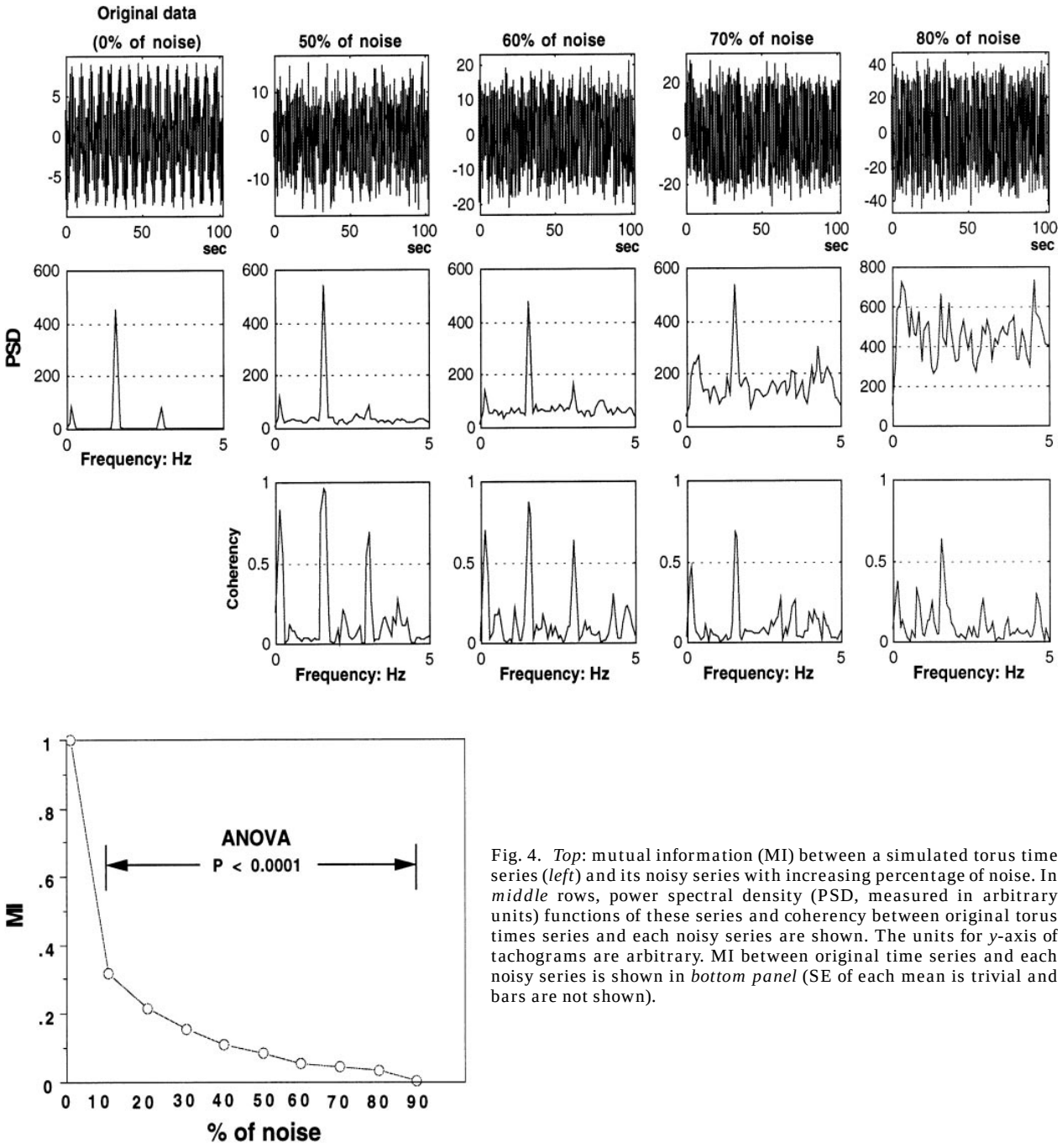

Fig. 4. *Top*: mutual information (MI) between a simulated torus time series (*left*) and its noisy series with increasing percentage of noise. In *middle* rows, power spectral density (PSD, measured in arbitrary units) functions of these series and coherency between original torus times series and each noisy series are shown. The units for *y*-axis of tachograms are arbitrary. MI between original time series and each noisy series is shown in *bottom panel* (SE of each mean is trivial and bars are not shown).

$I[x(t), y(t)]$ in which $y(t)$ contained 70% noise (0.047 ± 0.002) was taken as the threshold value to discriminate correlated from noncorrelated data. In particular, an MI value >0.088, which was the average of $I[x(t), y(t)]$ when $y(t)$ contained 50% noise, indicated the strong correlation between them. This result would provide a measure to assess the effect of noise on MI between an original series and the noisy series. With an increasing percentage of noise, the main peaks in the spectrum of the noisy torus $y(t)$ that were consistent with those in the spectrum of $x(t)$ became obscure and the MI value between them decreased. This suggests that the high MI values corresponded to the fluctuations pertaining to these main peaks. Hence, in cases in which two time series show several consistent peaks in their spectra and have a high MI value, the respective fluctuations pertaining to these main peaks would be strongly correlated with each other between these time series.

In APPENDIX B, we describe two simulations. One simulation shows that an MI value of zero means that two time series are neither linearly nor nonlinearly correlated at all. The other simulation shows the reliability of MI analysis for detecting the time delay between two torus series.

Simulation 2. Suppose that $x(t)$ and $y(t)$ are both formed from the same purely random process $z(t)$,

which has a mean of zero and a variance of σ_z^2, by

$$x(t) = z(t)$$

$$y(t) = 0.5z(t - 1) + 0.5z(t - 2)$$

The data length of these series was 16,384 (2^{14}) samples. The sampling rate was 1 Hz. For coherency analysis, these data were sectioned using a 50% overlap, and auto- and cross-spectra estimates were optimized by ensemble averaging 127 data epochs of 256 points. Figure 5 shows the randomness of $x(t)$ and $y(t)$ and indicates that the coherency spectrum $C(\omega)$ is almost constant and equal to one. In fact, the coherency spectrum is given by $C(\omega) = 1$ for all ω in (0, 0.5), after the application of some algebra using the definition of the coherency spectrum. A value of unity indicates a perfectly linear relationship between $x(t)$ and $y(t)$ at any frequency. The time series $y(t)$ was linearly correlated with $x(t)$, and this explains why there was perfect correlation between the components of the two processes at any given frequency. The coherency spectrum faithfully reflected the perfect correlation between $x(t)$ and $y(t)$. On the other hand, the MI value between $x(t)$ and $y(t)$ equaled unity and likely reflected the perfect correlation between them. This example indicates that even if $x(t)$ and $y(t)$ are noise processes, both coherency and MI can quantify the perfect correlation between them faithfully if they are linearly correlated.

Simulation 3. We examined another case in which $x(t)$ and $y(t)$ were not linearly correlated at all. The time series $x(t)$ was a noise process as shown in Fig. 6, where $1 \leq x(t) \leq 16{,}384$; if $t_1 \neq t_2$, then $x(t_1) \neq x(t_2)$. The time series $y(t)$ was generated by one-to-one relation from the *X-Y* plot of Fig. 6. The sampling rate was 1 Hz. The region of the *X-Y* plot is divided into 16 subregions. In each of the four subregions denoted as *A*, *B*, *C*, and *D* (Fig. 6), $x(t)$ and $y(t)$ were perfectly linearly correlated. The data length of these series was 16,384 samples. The coherency spectrum was computed in the same manner as in Fig. 5. Coherency of $x(t)$ and $y(t)$ at any frequency was <0.05. Although this indicates that $x(t)$ and $y(t)$ were not linearly correlated at all, it provides no information as to whether they were nonlinearly correlated. On the other hand, the MI value between the series was just unity, indicating that $x(t)$ and $y(t)$ had a perfect correlation. This case demonstrates that the coherency method fails to detect correlation between two time series that are nonlinearly correlated.

Simulation 4. Using simulated data, we determined that the confidence of coherence depends on the number of data epochs. In the same manner as that shown in Fig. 6, $x(t)$ and $y(t)$ were not linearly correlated at all. The time series $x(t)$ was a noise process for which $1 \leq x(t) \leq 1{,}024$; if $t_1 \neq t_2$, then $x(t_1) \neq x(t_2)$. The time series $y(t)$ was generated by one-to-one relation from the *X-Y* plot of Fig. 7. The data length of these series was 1,024 samples. The sampling rate was 1 Hz. For coherency analysis, these data were sectioned without any over-

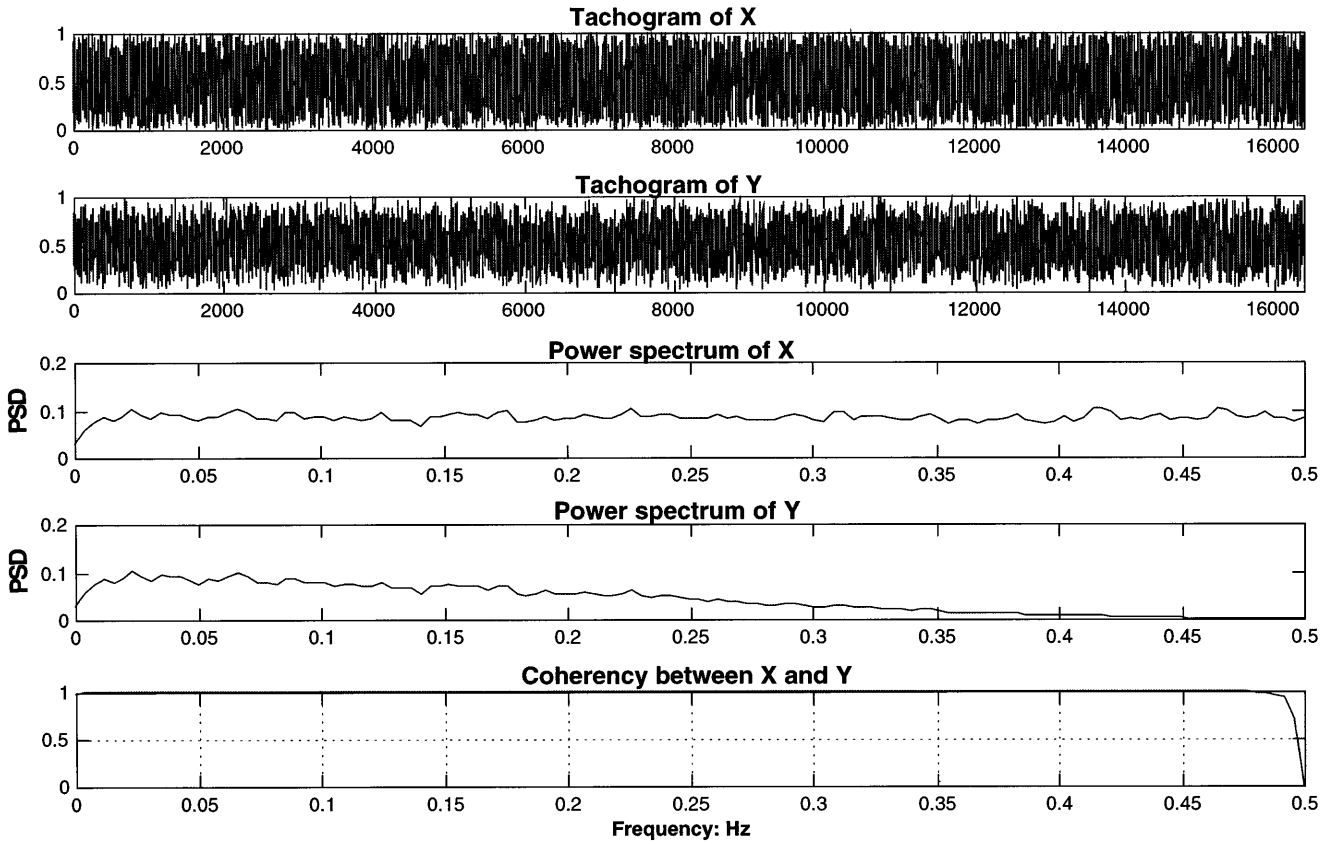

Fig. 5. Frequency domain analysis of 2 simulated random time series, *X* and *Y*, which are perfectly linearly correlated. PSD is measured in arbitrary units. The units for *x*-axis of tachograms are in seconds and the units for *y*-axis are arbitrary.

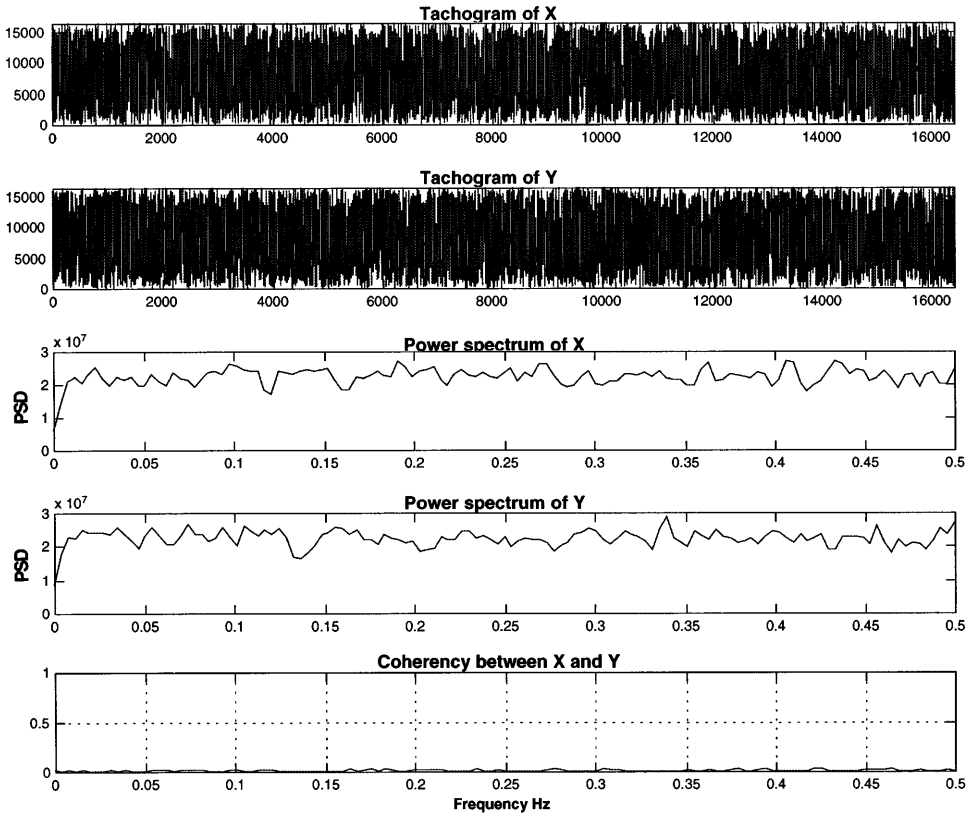

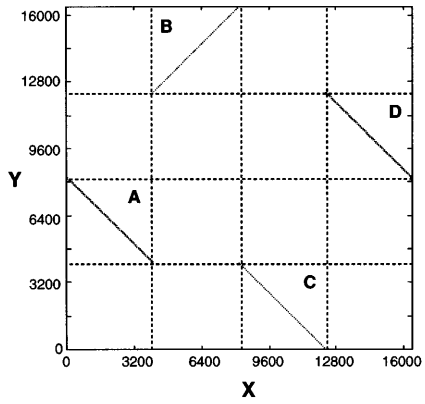

Fig. 6. Frequency domain analysis of 2 simulated random time series, X and Y, which are nonlinearly correlated. The time series $x(t)$ is a noise process shown in tachogram of X, where $1 \leq x(t) \leq 16{,}384$; if $t_1 \neq t_2$, then $x(t_1) \neq x(t_2)$. The units for x-axis of tachograms are in seconds and the units for y-axis are arbitrary. The time series $y(t)$ is generated by one-to-one relation from the X-Y plot (*bottom panel*). The region of the X-Y plot is divided into 16 subregions. In each of 4 subregions denoted by A, B, C, and D, $x(t)$ and $y(t)$ are perfectly linearly correlated. PSD is measured in arbitrary units. The units for both axes of the X-Y plot (*bottom*) are arbitrary.

lap, and auto- and cross-spectra estimates were optimized by ensemble averaging four data epochs of 256 points. For example, assume that a value of $C(\omega) = 0.5$ is estimated at a frequency of interest. The normalized random error of the coherence function estimate is then approximated by using the estimate $C(\omega)$ in place of the unknown true coherence as follows (Ref. 7, p. 311)

$$\frac{\sqrt{2}[1 - C(\omega)]}{\sqrt{C(\omega)}\sqrt{n}} = 0.5$$

where $C(\omega) = 0.5$ and $n = 4$ data epochs. Hence, an approximate 95% confidence interval for the true value of coherence at this frequency is between zero and one. This formula indicates that the normalized random error of the coherence function estimate approaches zero as either $n \rightarrow \infty$ or $C(\omega) \rightarrow 1$. Therefore, we took the data length in *simulation 3* to be 16 times as large as that in this simulation. In *simulation 3* the data were sectioned with the use of a 50% overlap, and the number of data epochs was 127. Eighteen frequencies can be counted between 0 and 0.5 Hz at which the coherence value exceeds 0.5 in Fig. 7, whereas no such frequencies are present in Fig. 6. Hence, these results indicate that the confidence of coherence computed by coherency analysis depends on the number of data epochs. For coherency analysis of the experimental data, the number of data epochs was at least nine. If a coherency value is then estimated to be 0.5 at a frequency of interest, an ~95% confidence interval for the true value of coherence is between 0.2 and 0.8. Therefore, coherency values >0.5 were considered significant.

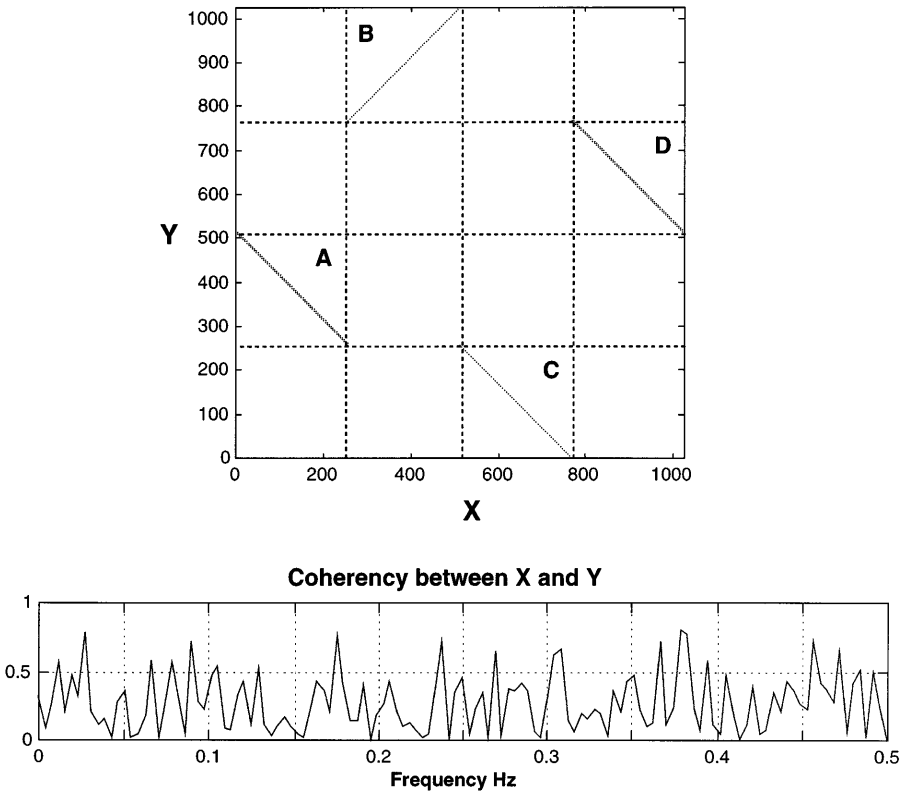

Fig. 7. Coherency analysis of 2 simulated random time series, X and Y, which are nonlinearly correlated in the same manner as in Fig. 6. Data length of 1,024 was one-sixteenth of that in Fig. 6. The time series $x(t)$ is a noise process, where $1 \leq x(t) \leq 1{,}024$; if $t_1 \neq t_2$, then $x(t_1) \neq x(t_2)$. The time series $y(t)$ is generated by one-to-one relation from the X-Y plot. PSD is measured in arbitrary units. The units for both axes of the X-Y plot are arbitrary.

Experimental Data

Figure 8 shows the representative tachograms and power spectra of HR, RSNA, and BP during the natural heart state in a dog. The coherency spectra and phase-angle spectra between each two variables are also shown in Fig. 8. The frequency of the maximum peak power in these power spectra is almost the same (0.12 Hz). The coherency values between HR and BP and between RSNA and BP were >0.5 at 0.12 Hz, indicating that they are significantly linearly correlated with each other, whereas coherency between HR and RSNA was not significant. In the time-domain analysis, the correlation coefficient between HR and BP, that between RSNA and BP, and that between HR and RSNA were -0.17, 0.25, and -0.19, respectively. Although these correlation coefficients were small, the hypothesis of zero correlation for each pair was rejected (Ref. 7, p. 101). On the other hand, the maximum MI values between these variables were I_{max}(HR, RSNA) = 0.25, I_{max}(HR, BP) = 0.17, and I_{max}(RSNA, BP) = 0.13. These values indicate that these variables have mutual dependence on one another and, especially, that HR and RSNA have a very strong correlation. From the cross-spectrum phase-angle estimates at 0.12 Hz, RSNA led HR by 2.9 $\pm$ 0.8 s, BP led HR by 2.1 $\pm$ 0.3 s, and RSNA led BP by 0.9 $\pm$ 0.6 s. These standard deviations of time delays at the frequency were estimated with the use of a formula to compute those of the phase angles (Ref. 7, p. 301). From MI analysis, RSNA led HR by 2.1 s, BP led HR by 2.0 s, and RSNA led BP by 0.5 s. The time delay between each pair of these variables as estimated by MI analysis was within its range as estimated by phase-angle analysis, and the relationship between them with respect to leading was the same.

Figures 9 and 10 show tachograms, power spectra of RSNA and BP, and coherency spectra between RSNA and BP during the artificial heart states with pacing rates of 60 and 160 beats/min, respectively, in the same dog as in Fig. 8. With a pacing rate of 60 beats/min, the low-frequency peak in the RSNA spectrum was consistent with that in the BP spectrum. The considerable components appeared in a broader frequency band of spectra of RSNA and BP for a pacing rate of 160 beats/min compared with those for a pacing rate of 60 beats/min. The coherency value between RSNA and BP at 0.12 Hz was higher with a pacing rate of 60 beats/min than with a pacing rate of 160 beats/min. The correlation coefficient between RSNA and BP was higher with a pacing rate of 60 beats/min than with a pacing rate of 160 beats/min (-0.58 and 0.32, respectively). These findings indicate that the linear correlation between RSNA and BP decreased at a higher pacing rate. Because HR was constant during the artificial heart state, only I(RSNA, BP) was calculated. I_{max}(RSNA, BP) at pacing rates of 60 beats/min and 160 beats/min were 0.16 and 0.08, respectively. This indicates that the correlation between RSNA and BP decreased with an increasing pacing rate. RSNA and BP, however, were significantly correlated even with a pacing rate of 160 beats/min. At a pacing rate of 60 beats/min, RSNA led BP by 3.6 $\pm$ 0.2 s according to the cross-spectrum phase-angle estimates at 0.12 Hz, whereas RSNA led BP by 0.6 s according to MI analysis. At a pacing rate of 160 beats/min, the coherencies

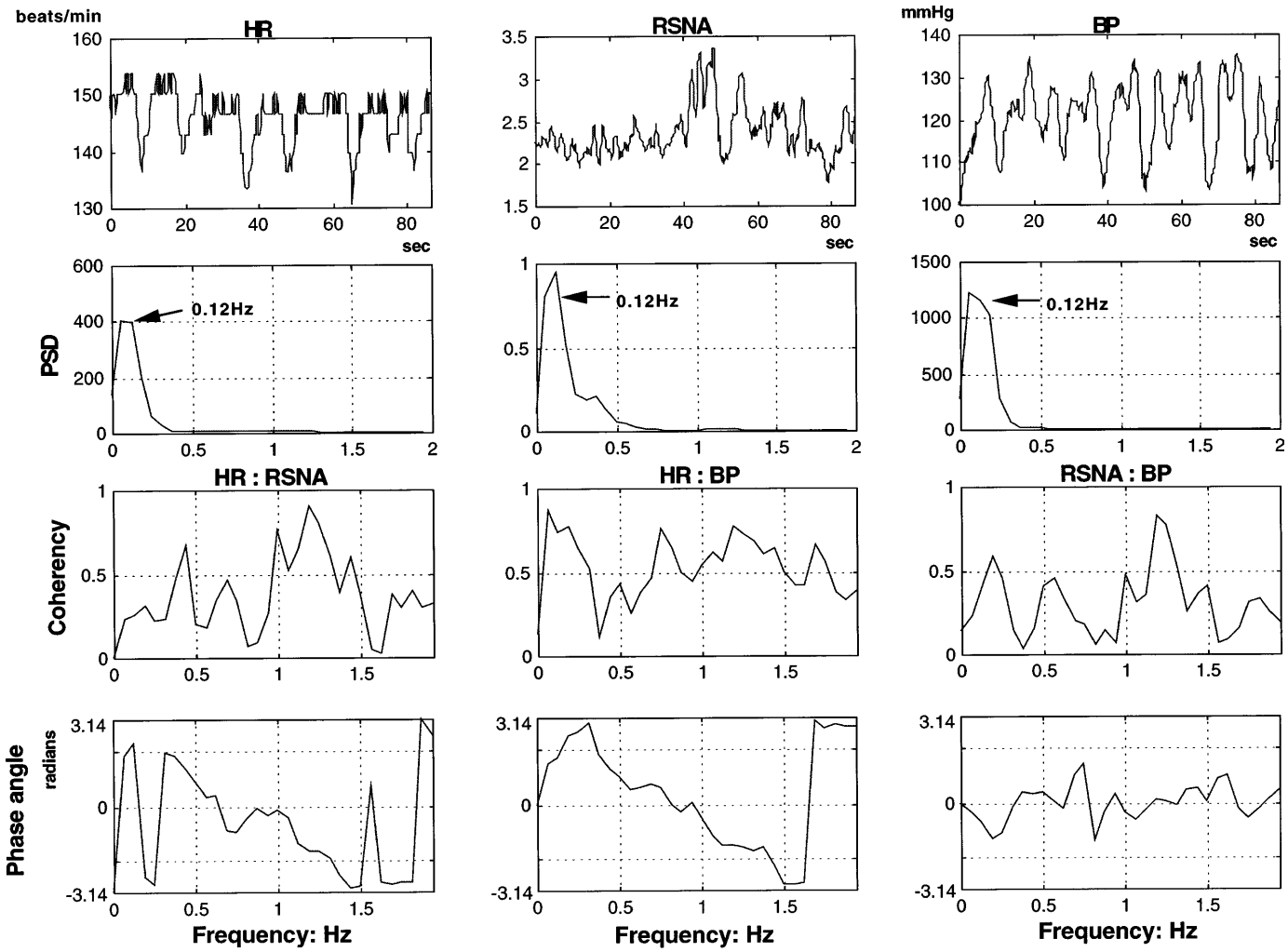

Fig. 8. Typical example of results of frequency analysis of heart rate (HR), RSNA, and BP during natural heart state in a dog. Units of measure for RSNA are arbitrary; units for PSD of HR and BP are $(\text{beats/min})^2/\text{Hz}$ and mmHg^2/Hz, respectively. HR:RSNA, coherency spectrum between HR and RSNA; HR:BP, coherency spectrum between HR and BP; RSNA:BP, coherency spectrum between RSNA and BP.

between RSNA and BP at some frequencies >0.25 Hz were significant and the phase angles at the respective frequencies were roughly zero radian. These results were compatible with those from MI analysis in that they were strongly correlated and the time delays between them were <0.25 s.

During the control state, I_{max}(HR, RSNA) > I_{max}(HR, BP) > I_{max}(RSNA, BP) as shown by ANOVA ($P < 0.05$) (Fig. 11). This indicates that the correlation between HR and RSNA is stronger than that between HR and BP and that between RSNA and BP. I_{max}(RSNA, BP) was significantly larger at a pacing rate of 60 beats/min than at the other pacing rates (80–160 beats/min) or in control ($P < 0.05$) (Fig. 12).

The time delay of HR and RSNA [T_{max}(HR, RSNA)] was significantly different from T_{max}(HR, BP) and T_{max}(RSNA, BP) during the control state ($P < 0.05$) (Fig. 13). These results show that RSNA leads BP, BP leads HR, and RSNA leads HR during the control state. The values of T_{max}(RSNA, BP) were significantly different at the pacing rates (60–160 beats/min) or in control ($P < 0.05$) (Fig. 14).

DISCUSSION

In this study we proposed and tested the MI technique to assess correlation between two time series. In the case in which the MI value between a pair of variables is >0.088, which is the average of $I[x(t), y(t)]$ where $y(t)$ contains 50% noise, it is indicated that these variables are correlated even if they are contaminated by noise. On the other hand, some researchers took a coherency value of 0.5 as the threshold value above which there is a significant correlation between oscillations in different variables (28, 31). Although the confidence of coherence can be enhanced by dividing data into multiple epochs and ensemble averaging, it might be practically difficult to achieve the normalized random error, which equals 0.1. For example, when a value of coherence equals 0.5, >100 epochs are necessary to achieve ~95% confidence intervals (7). This reduces resolution because the length of the data epoch determines the limits of the low-frequency resolution. However, the coherency analysis might have the advantage of gauging the linear correlation between two time

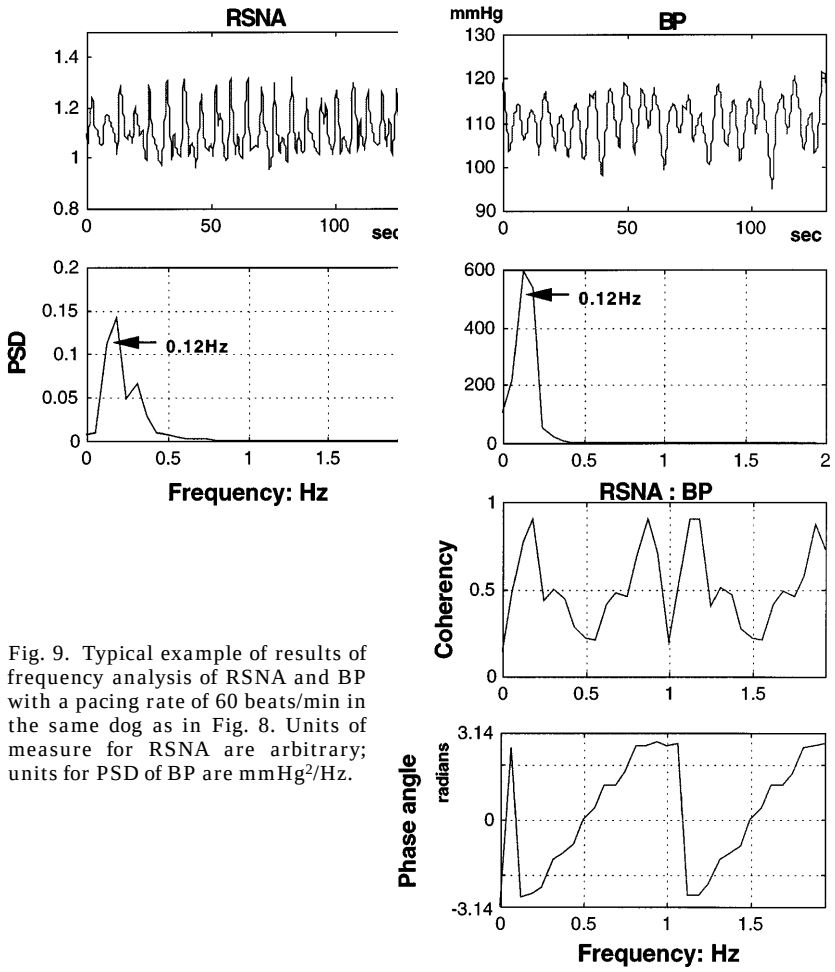

Fig. 9. Typical example of results of frequency analysis of RSNA and BP with a pacing rate of 60 beats/min in the same dog as in Fig. 8. Units of measure for RSNA are arbitrary; units for PSD of BP are $mmHg^2/Hz$.

series at any frequency. Hence, to quantify the relationship between two time series $x(t)$ and $y(t)$, coherency analysis as well as MI analysis should be used. Although the MI value does not quantify the relationship between the time series at a frequency of interest, it can quantify the nonlinear as well as linear dependence between them. In particular, the findings in *Simulation 1* indicate that, in the case of two time series showing several consistent peaks in their spectra and a high MI value, the respective fluctuations pertaining to these main peaks would be strongly correlated with each other between these time series.

During the control state, the frequency of the maximum power in the HR spectrum was the same as that of the maximum power in the RSNA spectrum. Moreover, the MI value between them was 0.25, indicating that they had a strong correlation. On the other hand, the peak power at 0.12 Hz in the RSNA spectrum was in the frequency range from 0.04 to 0.15 Hz, which has been defined as the low-frequency (LF) component in the power spectra of heart rate variability in humans and dogs (2, 27). The high-frequency component, from 0.15 to 0.4 Hz, has been considered to reflect the parasympathetic activity modulated by respiration. Recently, there have been some debates about whether the LF component reflects the fluctuation of sympathetic activity (28) or not (1, 6, 10). However, the frequency of the peak power was 0.12 Hz in both the HR and the RSNA spectra and I_{max}(HR, RSNA) was high (0.273 ± 0.022). According to the analysis in *Simulation 1*, these findings suggest that the LF component in the HR spectrum is modulated at least by the sympathetic activity.

Gebber and colleagues (16, 33) reported that a rhythmic fluctuation in the LF range persisted after denervation of all cardiovascular nerves. This suggests that the rhythmic discharge of the peripheral sympathetic nerve might result from a sympathetic rhythm of central origin that is normally entrained to the cardiac cycle by the pressor receptor input (35). To examine this hypothesis, we thought that the artificial heart model might be useful. If the cardiovascular regulatory system causes the rhythmic fluctuations of hemodynamic parameters through the natural heart, sympathetic nerve activity should not cause rhythmic fluctuations with the total artificial heart. The rhythmic fluctuations (0.12 Hz) of RSNA and BP were observed in a pacing rate of 60 beats/min (1 Hz). It is considered that these fluctuations are spontaneous because the rate of the fluctuations was different from the pacing rate. With this finding, the high values of I_{max}(RSNA, BP) suggest that these cyclic fluctuations are correlated strongly and are not induced by driving the artificial heart.

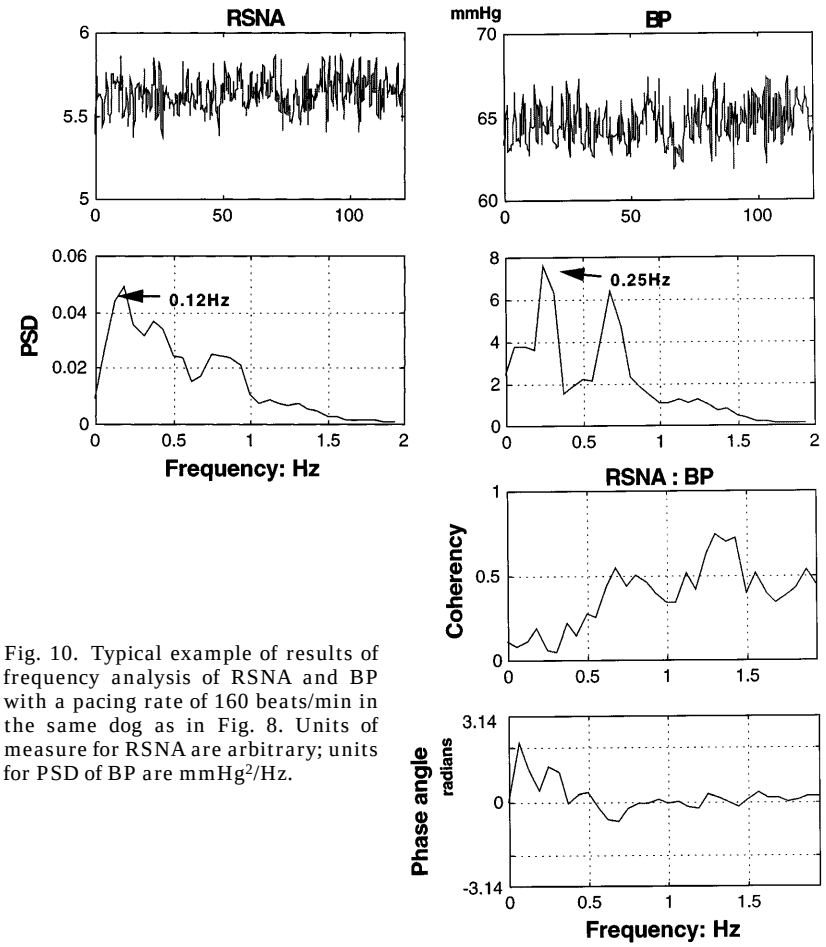

Fig. 10. Typical example of results of frequency analysis of RSNA and BP with a pacing rate of 160 beats/min in the same dog as in Fig. 8. Units of measure for RSNA are arbitrary; units for PSD of BP are $mmHg^2/Hz$.

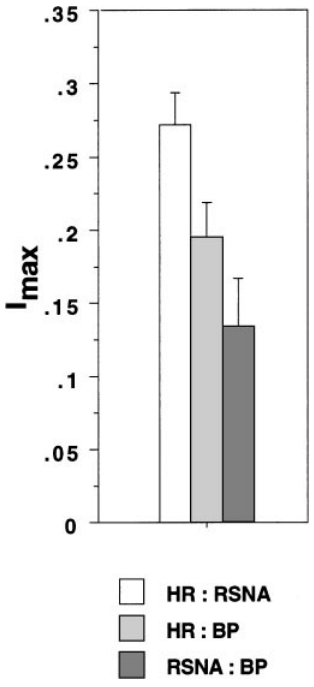

Fig. 11. Comparison of maximum values of mutual information (I_{max}) during natural heart state by ANOVA ($n = 7$). Maximum value of $I(T)$ between HR(t) and RSNA($t + T$), where T is time delay from -5 to 5 s, is denoted by I_{max}(HR, RSNA). $P < 0.05$.

Using coherency analysis, Brown et al. (10) have reported that sympathetic interactions are more reliably reflected in the BP power spectrum than in the HR spectrum in the conscious rat (10). Indeed, Fig. 8 shows that the coherence between RSNA and BP was stronger than that between RSNA and HR in the LF band. We consider that these coherencies might reflect only the linear correlations between the series. In the present study the MI values among HR, RSNA, and BP during control indicate that the correlation between HR and RSNA is stronger than that between HR and BP and that between RSNA and BP. This might be because the sinus node is affected by efferent sympathetic nerve directly, although it responds to both sympathetic and vagal inputs.

We calculated the time delay of each pair of signals derived from the HR, RSNA, and BP signals by regarding a time delay at which the maximum MI value between the signals was given as a physiological delay. Such a time delay T does not indicate a time delay between two time series at a certain frequency of fluctuations originating from respective physiological inputs, for instance, sympathetic or vagal input, but instead means that one of these time series is most strongly correlated with the time series that is delayed for the time delay T from the other time series. The results on detection of the time delay between two torus series showed the superiority of MI analysis to coher-

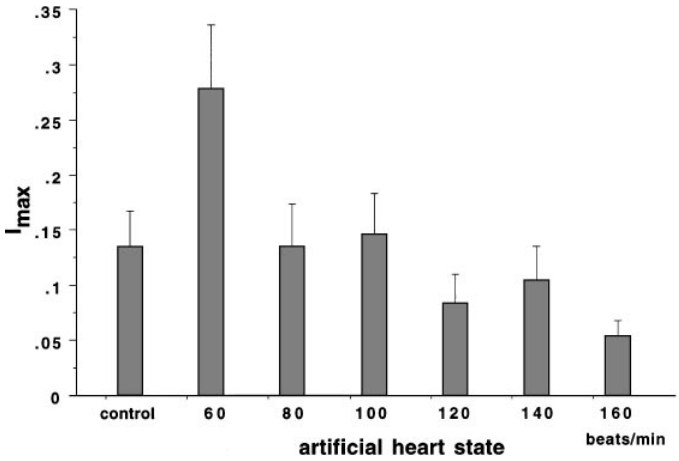

Fig. 12. Comparison of I_{max}(RSNA, BP) between control and total artificial heart states with pacing rates from 60 to 160 beats/min by ANOVA ($n = 7$). $P < 0.05$.

ency analysis. However, we must be very careful in interpreting the delay relations between these parameters because, during closed-loop operation of the control state, the relationship between HR and BP reflects both the feedback from BP to HR through the baroreflex and the moderating effect of HR on this response by changing BP through changes in cardiac output. Moreover, efferent sympathetic and vagal activities directed to the sinus node are characterized by discharge largely synchronous with each cardiac cycle that can be modulated by central (vasomotor and respiratory centers) and peripheral (oscillation in arterial pressure and respiratory movements) oscillators (23). These oscillators generate rhythmic fluctuation in efferent neural discharge and construct regulatory feedback loops. Although our results are difficult to account for precisely, they suggest that RSNA leads BP, BP leads HR, and RSNA leads HR during the control state in anesthetized dogs. Our results are compatible with the findings reported by Pagani et al. (27); however, there have been

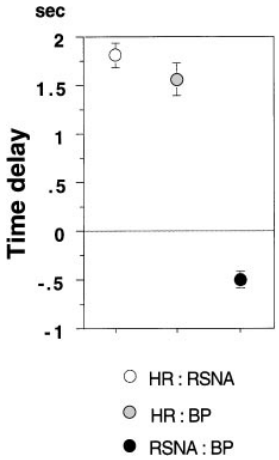

Fig. 13. Comparison of time delay T_{max} among HR, RSNA, and BP during control state by ANOVA ($n = 7$). $T_{max}(S, Q)$ is defined as time delay at which maximum mutual information value of $I(T)$ between S and Q ($-5 \leq T \leq 5$ s) is given. If $T_{max}(S, Q)$ is negative, then S leads Q. If $T_{max}(S, Q)$ is positive, then vice versa. $P < 0.05$.

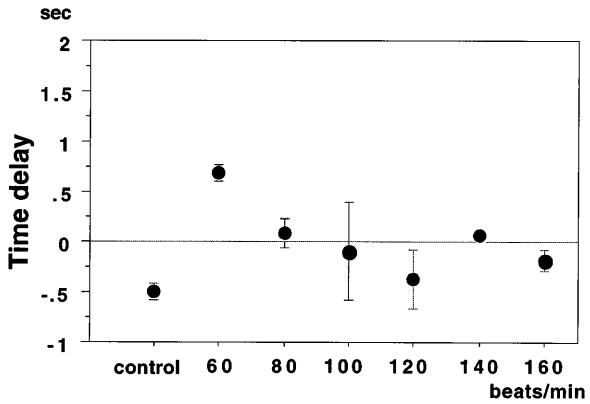

Fig. 14. Comparison of T_{max}(RSNA, BP) between control and total artificial heart states with pacing rates from 60 to 160 beats/min by ANOVA ($n = 7$). $P < 0.05$.

only a few reports available regarding the physiological delay between these parameters (31).

Perhaps the most difficult finding to explain is the small lags between RSNA and BP during the artificial heart state with pacing rates >60 beats/min. The demonstration in other studies (10, 12) that sympathetic activity can follow respiration has suggested that sympathetic nerve activity (SNA) can respond to rapid disturbances. Persson et al. (30) have reported that the phase lag of SNA and BP was roughly 0.2 s. Similarly, Fig. 2 shows that SNA can respond to the rapid increase of BP. On the other hand, there were considerable variabilities of RSNA and BP at a broader frequency band with a pacing rate of 160 beats/min than with a pacing rate of 60 beats/min (Figs. 9 and 10). With a pacing rate of 160 beats/min, the coherencies between RSNA and BP at some frequencies >0.25 Hz were significant, and the phase angles at the respective frequencies were roughly zero radian. These results were compatible with those from MI analysis in that they were strongly correlated and the time delays between them were <0.25 s. Although we should take the sampling frequency (8 Hz) into consideration to interpret "roughly zero" lags, these observations raise the possibility of a rapid response of RSNA to BP with an increasing pacing rate.

During the artificial heart state, I_{max}(RSNA, BP) was significantly larger with a pacing rate of 60 beats/min than with other pacing rates. This finding indicates that the fluctuation of sympathetic nerve is strongly correlated with that of BP with a pacing rate of 60 beats/min. I_{max}(RSNA, BP) decreased with increasing pacing rate. This might suggest that a response of the baroreflex system to BP depends on pacing rates of the artificial heart and that the response can hardly keep up with the increasing pacing rate. Thus we believe that the neurological effect of the total artificial heart must be considered when its driving conditions are selected.

Limitations

We should take effects of anesthesia on the cardiovascular control system into consideration. Most of the

gaseous anesthetic agents, including the nitrous oxide used in the present study, depress sympathetic activities in different regions of the sympathetic nervous system (13, 20). However, Keyl et al. (18) demonstrated, by means of spectral analysis of heart rate variability, that general anesthesia had no disadvantageous effects compared with local anesthesia on the perioperative cardiac autonomic tone during ophthalmic surgical procedures in otherwise healthy patients. Even if the effects of anesthesia on cardiac autonomic tone must be considered, we think that the correlation among HR, RSNA, and BP could be assessed in this study because the frequencies of peak power were consistent in the spectra of these parameters (Figs. 8 and 9). This is supported by Brown et al. (10), who found that anesthesia with pentobarbital lowered spectral power for HR, SNA, and BP but essentially did not change the coherence between SNA and BP.

In conclusion, MI analysis has many features that are advantageous in assessing the relationship between various cardiovascular variables. *1*) The method consists of probabilistic processes that do not require linearity of data and thus is applicable to the assessment of data generated not only by a linear system but also by a nonlinear one. *2*) MI analysis can sensitively quantify the relationship between two time series and assess a time delay of the interaction between them. *3*) The MI algorithm is simple and quick to compute. We applied MI analysis to quantify the correlation among HR, RSNA, and BP in dogs during the natural heart state and during the total artificial heart state. We conclude, from both theoretical and practical perspectives, that MI analysis has a potentially wide range of applications in studies of cardiovascular variation.

APPENDIX A

Mutual information is a measure of information theory. S denotes the whole system that consists of possible messages. $P_s(s)$ is the probability density at a message s. The average amount of information gained from a measurement that specifies s is the entropy H of a system

$$H(S) = -\int P_s(s) \log P_s(s) ds$$

where $H(S)$ is the quantity of surprise one should feel when reading the result of a measurement. If the logarithm is taken to the base two, H is in units of bits. We considered a general coupled system (S, Q) and asked, "Given that s has been measured and found to be s_i, what uncertainty is there in a

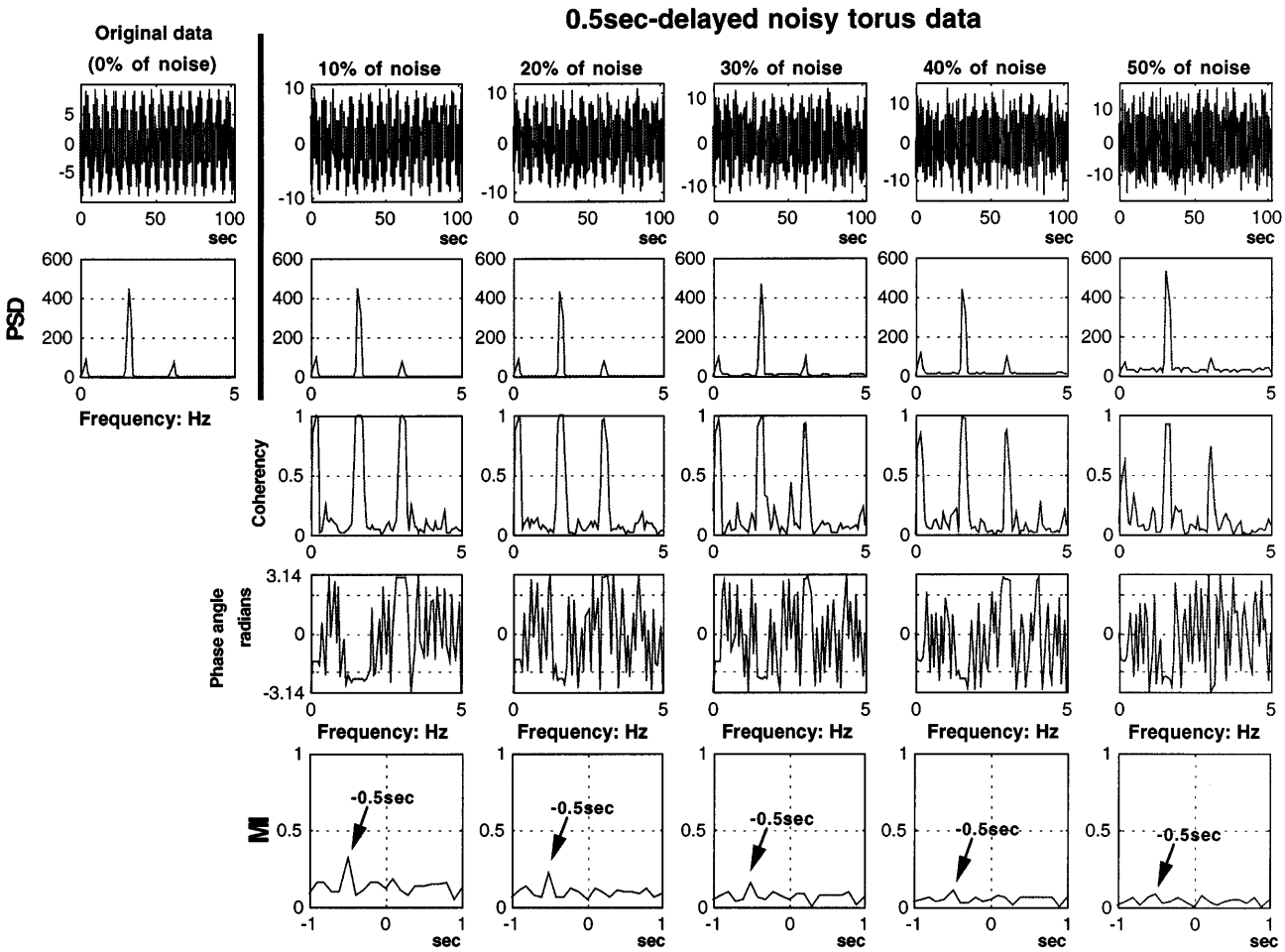

Fig. 15. Detection of a time delay between original torus series and 0.5-s-delayed noisy torus series by frequency analysis and MI analysis.

measurement of q?" The answer is

$$H(Q|s_i) = -\int P_{q|s}(q|s_i) \log P_{q|s}(q|s_i)\mathrm{d}q$$

$$= -\int [P_{sq}(s_i, q)/P_s(s_i)] \log [P_{sq}(s_i, q)/P_s(s_i)]\mathrm{d}q$$

where $P_{q|s}(q|s_i)$ is the probability of a measurement of q given the measured value of s_i and $P_{sq}(s, q)$ is the joint probability density at s and q. By averaging $H(Q|s_i)$ over s_i, the average uncertainty was obtained

$$H(Q|S) = \int P_s(s)H(Q|s)\mathrm{d}s$$

$$= -\int\int P_{sq}(s, q) \log [P_{sq}(s, q)/P_s(s)]\mathrm{d}s\mathrm{d}q$$

$$= H(S, Q) - H(S)$$

where

$$H(S, Q) = -\int\int P_{sq}(s, q) \log [P_{sq}(s, q)]\mathrm{d}s\mathrm{d}q$$

Hence, the amount that a measurement of s reduces the uncertainty of q is

$$I(Q, S) \equiv H(Q) - H(Q|S)$$

$$= H(Q) + H(S) - H(S, Q) = I(S, Q)$$

This is the mutual information. Individual entropies of continuous systems depend on coordinates, but this algorithm was developed to measure a coordinate-independent difference of entropies for the discrete case. We calculated values of mutual information between time series $x(t_i)$ and $y(t_i)$ according to an algorithm proposed by Fraser and Swinney (15). The data length is the power of two, that is, 2^n. $x(t_i)$ and $y(t_i)$ were changed into $s(t_i)$ and $q(t_i)$ in a fashion that preserves orderings, with the constraints that if $x(t_1) < x(t_2)$, then $s(t_1) < s(t_2)$ and $1 \leq s(t_i) \leq 2^n$ and with the same constraints for $q(t_i)$. We measured how dependent the values of $s(t)$ were on the values of $q(t)$. We defined a sequence of partitions of the (s, q) plane $(G_0, G_1, G_2, ..., G_m, ...)$ such that each partition is a rectangular grid of 4^m elements generated by dividing each axis into 2^m equiprobable segments. $R_m(K_m)$ denoted an element of G_m, where K_m is an index that takes one of 4^m possible values. Associated with the sequence of partitions G_m is a sequence i_m, which converges to $I(S, Q)$, where

$$i_m = \sum_{K_m} P_{sq}[R_m(K_m)] \log (P_{sq}[R_m(K_m)]/[P_s[R_m(K_m)]P_q[R_m(K_m)]])$$

$P_{sq}[R_m(K_m)]$ is estimated by $N[R_m(K_m)]/N_0$, where $N[R_m(K_m)]$ is the number of events observed in partition element $R_m(K_m)$ and N_0 is the total number of events observed. One representation of K_m is the ordered pair (i, j), where i indicates a range of s values and j indicates a range of q values. With the definition of $R_m(K_m)$

$$P_s[R_m(K_m)] = P_q[R_m(K_m)] = (1/2)^m$$

and

$$i_m = m \log (4) + \sum_{i,j=0} P_{sq}[R_m(i, j)] \log [P_{sq}[R_m(i, j)]]$$

The algorithm requires a recursive approach to the definition of $I(S, Q)$. These steps are iterated in areas in which P_{sq} has finer structure, yielding smaller partition elements where they are needed. When the number 2^m of equiprobable segments of each axis approaches the data length, i_m converges to $I(S, Q)$. Therefore, if $S = Q$, then $I(S, Q) = n$, where the data length is 2^n. The detailed algorithm is referred to in Ref. 15.

APPENDIX B

Simulation 5. To compare the results of our experimental data, we took the scalar data consisting of 1,024 random numbers as a time series $[r(t)]$ and measured how dependent the values of $r(t + T)$ are on the values of $r(t)$. The MI values of $[r(t), r(t + T)]$, where T was a time delay such that $0 \leq T \leq 10$, in a step of one, were all zero. This result faithfully reflected the perfectly random generation of these random numbers. Hence, the MI value zero indeed indicates that two time series are neither linearly nor nonlinearly correlated at all.

Simulation 6. Using the torus series in *simulation 1*, we examined the reliability of MI analysis to detect the time delay between the original data $x(t)$ and the 0.5-s-delayed noisy data $z(t)$ as

$$z(t) \equiv y(t + 0.5)$$

$$= [R_1 + R_2 \sin [2\pi f_2(t + 0.5) + \phi]] \sin [2\pi f_1(t + 0.5)] + \xi$$

$I(T) \equiv I[x(t), z(t + T)]$ were computed from an original torus series and a delayed noisy torus series 1,024 samples long containing 10–50% noise at T, which was between -1 and 1 s in a step of 0.1 s. For each percentage of noise, the coherency spectrum between $x(t)$ and $z(t)$ was computed in the same manner as that between $x(t)$ and $y(t)$. Figure 15 shows that the maximum value of $I(T)$ was at $T = -0.5$ s in all cases. This means that $x(t)$ leads $z(t)$ by 0.5 s. In frequency analysis, the time delay at 1.6 Hz, at which the maximum power appeared with the maximum coherency, was 0.25 s with $x(t)$ leading. Although it assumed that MI values relate primarily to the high power components of the signal, this result suggests that MI analysis can detect the time delay between two nonlinearly correlated processes in comparison with phase-angle analysis.

This work is partially supported by a Grant-in-Aid for Medical Research from the Alumni Association of Nippon Medical School and by a Grant-in-Aid from the Fukuda Foundation for Medical Technology.

This study was initiated at the 3rd Workshop, "Various Approaches to Complex Systems," held at the International Institute for Advanced Studies in Kyoto, Japan, 1996.

Address for reprint requests: M. Osaka, First Dept. of Internal Medicine, Nippon Medical School, Sendagi 1–1–5, Bunkyo-ku, Tokyo 113–8603, Japan.

Received 29 April 1998; accepted in final form 29 June 1998.

REFERENCES

1. **Ahmed, M. W., A. H. Kadish, M. A. Parker, and J. J. Goldberger.** Effect of physiologic and pharmacologic adrenergic stimulation on heart rate variability. *J. Am. Coll. Cardiol.* 24: 1082–1090, 1994.
2. **Akselrod, S., D. Gordon, J. B. Madwed, N. C. Snidman, D. C. Shannon, and R. J. Cohen.** Hemodynamic regulation: investigation by spectral analysis. *Am. J. Physiol.* 249 (*Heart Circ. Physiol.* 18): H867–H875, 1985.
3. **Akselrod, S., D. Gordon, F. A. Ubel, D. C. Shannon, A. C. Berger, and R. J. Cohen.** Power spectrum analysis of heart rate fluctuation: a quantitative probe of beat-to-beat cardiovascular control. *Science* 213: 220–222, 1981.
4. **Akutsu, T., and W. Kolff.** Permanent substitutes for valves and hearts. *ASAIO Trans.* 4: 230–232, 1958.
5. **Babloyantz, A., and A. Destexhe.** Is the normal heart a periodic oscillator? *Biol. Cybern.* 58: 203–211, 1988.

6. **Bailey, J. R., D. M. Fitzgerald, and R. J. Applegate.** Effects of constant cardiac autonomic nerve stimulation on heart rate variability. *Am. J. Physiol.* 270 (*Heart Circ. Physiol.* 39): H2081–H2087, 1996.
7. **Bendat, J. S., and A. G. Piersol.** *Random Data Analysis and Measurement Procedures* (2nd ed.). New York: Wiley, 1986.
8. **Berger, R. D., S. Akselrod, D. Gordon, and R. J. Cohen.** An efficient algorithm for spectral analysis of heart rate variability. *IEEE Trans. Biomed. Eng.* 33: 900–904, 1986.
9. **Berger, R. D., J. P. Saul, and R. J. Cohen.** Transfer function analysis of autonomic regulation. I. Canine atrial rate response. *Am. J. Physiol.* 256 (*Heart Circ. Physiol.* 25): H142–H152, 1989.
10. **Brown, D. R., L. V. Brown, A. Patwardhan, and D. C. Randall.** Sympathetic activity and blood pressure are tightly coupled at 0.4 Hz in conscious rats. *Am. J. Physiol.* 267 (*Regulatory Integrative Comp. Physiol.* 36): R1378–R1384, 1994.
11. **Butler, G. C., Y. Yamamoto, and R. L. Hughson.** Fractal nature of short-term systolic BP and HR variability during lower body negative pressure. *Am. J. Physiol.* 267 (*Regulatory Integrative Comp. Physiol.* 36): R26–R33, 1994.
12. **Cerutti, C., M. P. Gustin, C. Z. Paultre, M. Lo, C. Julien, M. Vincent, and J. Sassard.** Autonomic nervous system and cardiovascular variability in rats: a spectral analysis approach. *Am. J. Physiol.* 261 (*Heart Circ. Physiol.* 30): H1292–H1299, 1991.
13. **Ebert, J. J., and J. P. Kampine.** Nitrous oxide augments sympathetic outflow; direct evidence from human peroneal nerve recordings. *Anesth. Analg.* 69: 444–449, 1989.
14. **Eckberg, D. L., C. Nerhed, and B. G. Wallin.** Respiratory modulation of muscle sympathetic and vagal cardiac outflow in man. *J. Physiol. (Lond.)* 365: 181–196, 1985.
15. **Fraser, A. M., and H. L. Swinney.** Independent coordinates for strange attractors from mutual information. *Phys. Rev. A* 33: 1134–1140, 1986.
16. **Gebber, G. L.** Central oscillators responsible for sympathetic nerve discharge. *Am. J. Physiol.* 239 (*Heart Circ. Physiol.* 8): H143–H155, 1980.
17. **Hodgkin, A. L., and A. F. Huxley.** A quantitative description of membrane current and its application to conduction and excitation in nerve. *J. Physiol. (Lond.)* 117: 500–544, 1952.
18. **Keyl, C., P. Lemberger, A. W. Frey, M. Dambacher, and J. Hobbhahn.** Perioperative changes in cardiac autonomic control in patients receiving either general or local anesthesia for ophthalmic surgery. *Anesth. Analg.* 82: 113–118, 1996.
19. **Kobayashi, M., and T. Musha.** 1/*f* Fluctuation of heartbeat period. *IEEE Trans. Biomed. Eng.* 29: 456–457, 1982.
20. **Koizumi, K., A. Sato, A. Kaufman, and C. M. Brooks.** Studies of sympathetic neuron discharges modified by central and peripheral excitation. *Brain Res.* 37: 804–832, 1965.
21. **Mabuchi, K., H. Hayakawa, Y. Hirata, M. Iizuka, K. Imachi, T. Chinzei, H. Nozawa, Y. Abe, T. Yonezawa, M. Suzukawa, K. Imanishi, K. Atsumi, T. Sugimoto, and I. Fujimasa.** Suppression of the natriuretic effects of exogenous atrial natriuretic peptide in animals with total artificial hearts. *ASAIO Trans.* 37: M214–M216, 1991.
22. **Maeda, K., T. Chinzei, K. Imachi, K. Mabuchi, Y. Abe, T. Yonezawa, and K. Imanishi.** Predictive control by physical activity rate of a total artificial heart during exercise. *ASAIO Trans.* 34: 480–484, 1988.
23. **Malliani, A., M. Pagani, F. Lombardi, and S. Cerutti.** Cardiovascular neural regulation explored in the frequency domain. *Circulation* 84: 1482–1492, 1991.
24. **Nitta, S., Y. Katahira, T. Yambe, M. Tanaka, K. Kagawa, T. Hongo, N. Sato, and M. Miura.** Experimental and clinical evaluation of a sac-type ventricular assist device and drive system. In: *Artificial Heart 2: Proceedings of the 2nd International Symposium on Artificial Heart and Assist Devices, August 13–14, 1987, Tokyo, Japan*, edited by T. Akutsu. Tokyo: Springer-Verlag, 1988, p. 131–140.
25. **Osaka, M., H. Saitoh, H. Atarashi, and H. Hayakawa.** Correlation dimension of heart rate variability: a new index of human autonomic function. *Front. Med. Biol. Eng.* 5: 289–300, 1993.
26. **Osaka, M., H. Saitoh, T. Yokoshima, H. Kishida, H. Hayakawa, and R. J. Cohen.** Nonlinear pattern analysis of ventricular premature beats by mutual information. *Methods Inf. Med.* 36: 257–260, 1997.
27. **Pagani, M., F. Lombardi, S. Guzzetti, O. Rimoldi, R. Furlan, P. Pizzinelli, G. Sandrone, G. Malfatto, S. Dell'Orto, E. Piccaluga, M. Turiel, G. Baselli, S. Cerutti, and A. Malliani.** Power spectral analysis of heart rate and arterial pressure variabilities as a marker of sympatho-vagal interaction in man and conscious dog. *Circ. Res.* 59: 178–193, 1986.
28. **Pagani, M., N. Montano, A Porta, A. Malliani, F. M. Abboud, C. Birkett, and V. K. Somers.** Relationship between spectral components of cardiovascular variabilities and direct measures of muscle sympathetic nerve activity in humans. *Circulation* 95: 1441–1448, 1997.
29. **Palus, M.** Identifying and quantifying chaos by using information-theoretic functionals. In: *Time Series Prediction: Forecasting the Future and Understanding the Past*, edited by A. S. Weigend and N. A. Gershenfeld. Reading, MA: Addison-Wesley, 1994, p. 387–413.
30. **Persson, P. B., H. Stauss, O. Chung, U. Wittmann, and T. Unger.** Spectrum analysis of sympathetic nerve activity and blood pressure in conscious rats. *Am. J. Physiol.* 263 (*Heart Circ. Physiol.* 32): H1348–H1355, 1992.
31. **Saul, J. P., R. D. Berger, P. Albrecht, S. P. Stein, M. H. Chen, and R. J. Cohen.** Transfer function analysis of the circulation: unique insights into cardiovascular regulation. *Am. J. Physiol.* 261 (*Heart Circ. Physiol.* 30): H1231–H1245, 1991.
32. **Saul, J. P., R. F. Rea, D. L. Eckberg, R. D. Berger, and R. J. Cohen.** Heart rate and muscle sympathetic nerve variability during reflex changes of autonomic activity. *Am. J. Physiol.* 258 (*Heart Circ. Physiol.* 27): H713–H721, 1990.
33. **Taylor, D. G., and G. L. Gebber.** Baroreceptor mechanism controlling sympathetic nervous rhythms of central origin. *Am. J. Physiol.* 228: 1002–1013, 1975.
34. **Toda, K., E. Tatsumi, Y. Taenaka, T. Masuzawa, K. Miyazaki, T. Nakatani, Y. Baba, K. Eya, Y. Wakisaka, and H. Takano.** Influence of ventricular fibrillation on sympathetic nerve activity under biventricular bypass circulation. *Artif. Organs* 20: 143–146, 1996.
35. **Wurster, R. D.** Central nervous system regulation of the heart: an overview. In: *Nervous Control of Cardiovascular Function*, edited by W. C. Randau. Oxford, UK: Oxford University Press, 1984, p. 307–345.
36. **Yamamoto, Y., and R. L. Hughson.** On the fractal nature of heart rate variability in humans: effects of data length and beta-adrenergic blockade. *Am. J. Physiol.* 266 (*Regulatory Integrative Comp. Physiol.* 35): R40–R49, 1994.
37. **Yambe, T., S. Nitta, Y. Katahira, T. Sonobe, S. Naganuma, H. Akiho, S. Chiba, Y. Kakinuma, H. Hayashi, M. Tanaka, M. Miura, N. Satoh, H. Mohri, M. Yoshizawa, and H. Takeda.** Postganglionic sympathetic nerve activity with correlation to heart rhythm during left ventricular assistance. *Artif. Organs* 15: 212–217, 1991.
38. **Yambe, T., S. Nitta, S. Naganuma, Y. Kakinuma, K. Izutsu, H. Akiho, T. Naganuma, Y. Kikuchi, S. Kobayashi, N. Ohsawa, S. Nanka, M. Tanaka, T. Fukuju, M. Miura, N. Uchida, N. Sato, H. Mohri, S. Koide, and K. Abe.** Fluctuations of the sympathetic nerve discharges in animals without natural heartbeat. *Artif. Organs* 18: 775–780, 1994.